Variable stoichiometry among core ribosomal proteins

Nikolai Slavov[1,2,3], Stefan Semrau[3], Edoardo Airoldi[1,2], Bogdan A. Budnik[1] & Alexander van Oudenaarden[3]

[1]*Department of Statistics and FAS Center for Systems Biology,*

Harvard University, Cambridge, MA 02138, USA

[2]*Broad Institute of MIT and Harvard, Cambridge, MA 02142*

[3]*Hubrecht Institute, Royal Netherlands Academy of Arts and Sciences and University Medical Center Utrecht, Uppsalalaan 8, 3584 CT, Utrecht, The Netherlands*

Understanding the regulation and structure of the eukaryotic ribosome is essential to understanding protein synthesis and its deregulation in disease. Traditionally ribosomes are believed to have a fixed stoichiometry among their core ribosomal proteins (RPs), but recent experiments suggest a more variable composition[1–6]. Reconciling these views requires direct and precise quantification of RPs. We used mass-spectrometry to directly quantify RPs across monosomes and polysomes of budding yeast and mouse embryonic stem cells (ESC). Our data show that the stoichiometry among core RPs in wild-type yeast cells and ESC depends both on the growth conditions and on the number of ribosomes bound per mRNA. Furthermore, we find that the fitness of cells with a deleted RP-gene is inversely proportional to the enrichment of the corresponding RP in ribosomes bound to multiple mRNAs. Together, these findings support the existence of ribosomes with distinct protein composition and physiological function.

Traditionally eukaryotic ribosomes have been thought to have a fixed composition of 80 core RPs[1–3], some of which are represented by several paralogous RPs. Recent studies of eukaryotic ribosomes[7–12] have demonstrated that (i) genetic perturbations to the core RPs specifically affect the translation of some mRNAs and not others and (ii) mRNAs coding for core RPs are transcribed, spliced, and translated differentially across physiological conditions[13–17]. These results suggest the hypothesis[4–6] that, depending on the tissue type and the physiological conditions, cells can alter the stoichiometry among the core RPs comprising the ribosomes and thus in turn alter the translational efficiency of distinct mRNAs. However, differential RP–expression can reflect extra ribosomal functions[7,18,19]. Furthermore, polysomes (multiple ribosomes per mRNA) from different cell–lines

have similar core RP stoichiometries[20]. Thus, the variable RP–stoichiometry in the ribosomes of wild-type cells that is suggested by the ribosome specialization hypothesis remains unproven.

To measure whether the stoichiometry among RPs can change with growth conditions, we used velocity-sedimentation in sucrose-gradients to isolate fractions containing monosomes and polysomes from yeast cells grown in minimal media with either glucose or ethanol as the sole source of carbon and energy[21] (Fig. 1a). The proteins from individual fractions were spiked-in with known amounts of universal proteomics standard (UPS2) proteins, digested to peptides, labeled with tandem mass tags (TMT), and quantified on Orbitrap Elite based on the MS2 intensities of the TMT reporter ions[21]. The accuracy of estimated fold-changes for peptides can be gauged by the good agreement between the measured and the spiked-in fold-changes for UPS2 (Fig. 1b) that were measured simultaneously with the yeast RPs. The measured fold-changes for UPS2 peptides are about 12% smaller than expected from the spiked-in levels, as indicated by the 0.88 slope of the linear fit in Fig. 1c, most likely due to coisolation interference[22].

To quantify RP paralogs independently from one another, the fold-change of each RP was estimated as the median fold-change of its unique peptides, i.e., peptides whose sequences are found only in that RP. Our data have multiple high–confidence unique peptides for most RPs (Extended Data Fig. 1a, b) except for highly homologous paralogs. These quantified unique peptides allow estimating the relative RP levels in monosomes and polysomes collected from yeast grown in glucose or ethanol media (Fig. 1c). We systematically tested whether the variability in the estimated RP levels (Fig. 1c) reflects stoichiometry differences among the RPs or other factors and

artifacts, such as noise in the MS measurements, a differential distribution of nascent RP polypeptides among monosomes and polysomes, posttranslational modifications (PTMs) of the RPs, and the presence of 90S ribosomal biogenesis particles[23]. These factors are unlikely to contribute significantly to the data in Fig. 1c since the majority of RP fold-changes that are estimated from multiple unique peptides differ by 10 % or less (Extended Data Fig. 1c, d and Supplementary Discussion) and the 90S particles are less abundant than the mature ribosomes (Extended Data Fig. 2 and Supplementary Discussion).

We find that the relative RP levels depend on two factors: the carbon source in the growth media and the number of ribosomes per mRNA (Fig. 1c). The RP levels that are higher in glucose compared to ethanol also tend to increase with the number of ribosomes per mRNA (Fig. 1c). Importantly, the RP composition of trisomes in ethanol, Eth (iii), is more similar to the composition of monosomes than to tetrasomes. This observation shows that polysomes (3 ribosomes per mRNA) may have similar RP composition to monosomes, suggesting that the RP composition of monosomes is not necessarily indicative of a non–functional state.

To explore the extent to which the RP variability reflects paralogous RPs substituting for each other, we separately plotted the relative levels of RPs without paralogs (Fig. 1d) and of paralogous RP pairs (Fig. 1e). The levels of RPs without paralogs (Fig. 1d) vary similarly to the levels of all RPs (Fig. 1c), indicating that exchange among paralogous RPs is not the sole reason for the variable RP–stoichiometry. Furthermore, while the levels of some paralogs, such as Rpl37ap and Rpl37bp, are anticorrelated and consistent with paralog–exchange, the levels of other paralogs,

such as Rpl17ap and Rpl17bp, are positively correlated and inconsistent with paralog–exchange across the analyzed ribosomes (Fig. 1e). The correlations between all paralogous pairs that we can confidently quantify based on unique peptides alone indicate similar distribution between positively and negatively correlated paralogous pairs (Fig. 1f).

Having found variability in the stoichiometry among yeast RPs, we sought to test its generality. We separated the ribosomes of exponentially growing mouse ESC on sucrose gradients (Fig. 2a) and quantified the core RPs, as annotated by Swiss–Prot, across different fractions corresponding to the number of ribosomes per mRNA (Fig. 2b). As in yeast, we observe significant variation in the stoichiometry among the mouse RPs depending on the number of ribosomes bound per mRNA. Furthermore, the ratios between the polysomal and monosomal levels of mouse RPs correlate to the corresponding ratios for their yeast orthologs (Fig. 2c; p-value < 0.03), suggesting that the RP-stoichiometry differences between monosomes and polysomes are conserved across yeast and mouse.

Next, we tested the variability among RPs and its phenotypic consequences by independent fitness measurements. Our observation that the RP stoichiometry depends on the number of ribosomes bound per mRNA parallels the observation that the translational activity per ribosome increases with the number of ribosomes bound per mRNA[24,25]. We therefore hypothesized that genetic deletions of RPs enriched in the more active ribosomes – as compared to RPs enriched in less active ribosomes – may result in a larger decrease of the translation rate and thus lower fitness. To test this hypothesis, we computed the correlation (Fig. 3a) between the fitness (in ethanol medium)

of yeast strains with single RP-gene deletions[26] and the corresponding relative RP levels measured in the tetra-ribosomal fraction (4 ribosomes per mRNA). Consistent with our hypothesis, the fitness of strains lacking RP-genes is inversely proportional to the relative levels of the corresponding RPs in the tetra-ribosomes (Fig. 3a). Extending this correlation analysis to the RP-levels in all sucrose fractions from both glucose and ethanol (Fig. 1c) results in a correlation pattern (Fig. 3b) that further supports our hypothesis by showing the opposite dependence for fractions with fewer ribosomes per mRNA: the fitness of strains lacking RP-genes is proportional to the relative levels of the corresponding RPs in fractions with fewer ribosomes per mRNA (Fig. 3b). This correlation pattern holds both for ethanol and for glucose carbon sources. To mitigate possible artifacts in the fitness data[26] due to potential chromosome duplications in the deletion strains, we computed the correlations between the levels and the fitness of RP-deletion strains only for RPs without paralogs (thus unlikely to be affected by chromosome duplication) and found much higher magnitudes of the correlations (Fig. 3a, c). This result suggests that the variability in the RP stoichiometry is not limited to paralogous RPs substituting for each other.

We extended our fitness analysis from yeast to mouse using the published depletion data from CRISPR knockouts in human ESC (HUES62)[27]. We identified the closest mouse orthologs of each human RP with deletion data by BLAST alignment (Fig. 3d) and correlated the fitness of human ESC lacking the human RP orthologs to the RP levels across sucrose fractions that we measured (Fig. 2b). The correlation pattern (Fig. 3e) is similar to the one in yeast (Fig. 3a-c) and highly significant (false discovery rate (FDR) $< 0.1\%$). This pattern indicates that the fitness of ESC lacking RP-genes is directly proportional to the relative RP levels in monosomes

and inversely proportional to the relative RP levels in polysomes. The magnitude of this inverse proportionality increases with the number of ribosomes per mRNA (Fig. 3e), consistent with our hypothesis. The fact that the fitness of human ESC lacking RPs correlates significantly to the levels of the corresponding mouse orthologous RPs suggests that the variability of the RP stoichiometry and its biological function are likely conserved across mouse and human. The magnitude of this correlation increases significantly when the correlation is computed based only on orthologs whose sequences are over 80% identical between mouse and human (Fig. 3e), providing further evidence for the conserved fitness consequences of the altered RP stoichiometry.

Pioneering experiments performed in the 1960's established that the rate of incorporating ^{14}C-leucine in proteins per ribosome increases along the sucrose gradient as the number of ribosomes bound per mRNA increases[24,25]. The increasing translational activity across sucrose gradients[24,25] parallels both our findings of altered RP stoichiometry across sucrose gradients (Fig. 2b) and the correlation of the altered RP stoichiometry to the fitness effects of mammalian RP deletions (Fig. 3e). These parallels can be explained by the expectation that the higher the translational activity of a ribosome, the higher the fitness cost of its perturbation in rapidly growing stem cells. The key factor required by this expectation is the variable ribosomal composition that we measured. The variable RP stoichiometry in the absence of external perturbations suggests that cells use variable RP composition of their ribosomes as a regulatory mechanism of protein translation.

1. Warner, J. R. The economics of ribosome biosynthesis in yeast. *Trends in biochemical sciences* **24**, 437–440 (1999).

2. Ben-Shem, A., Jenner, L., Yusupova, G. & Yusupov, M. Crystal structure of the eukaryotic ribosome. *Science* **330**, 1203–1209 (2010).

3. Ben-Shem, A. *et al.* The structure of the eukaryotic ribosome at 3.0 Å resolution. *Science* **334**, 1524–1529 (2011).

4. Mauro, V. P. & Edelman, G. M. The ribosome filter hypothesis. *Proceedings of the National Academy of Sciences* **99**, 12031–12036 (2002).

5. Gilbert, W. V. Functional specialization of ribosomes? *Trends in biochemical sciences* **36**, 127–132 (2011).

6. Xue, S. & Barna, M. Specialized ribosomes: a new frontier in gene regulation and organismal biology. *Nature Reviews Molecular Cell Biology* **13**, 355–369 (2012).

7. Mazumder, B. *et al.* Regulated release of L13a from the 60S ribosomal subunit as a mechanism of transcript-specific translational control. *Cell* **115**, 187–198 (2003).

8. Komili, S., Farny, N. G., Roth, F. P. & Silver, P. A. Functional specificity among ribosomal proteins regulates gene expression. *Cell* **131**, 557–571 (2007).

9. Kondrashov, N. *et al.* Ribosome-mediated specificity in Hox mRNA translation and vertebrate tissue patterning. *Cell* **145**, 383–397 (2011).

10. Horos, R. *et al.* Ribosomal deficiencies in diamond-blackfan anemia impair translation of transcripts essential for differentiation of murine and human erythroblasts. *Blood* **119**, 262–272 (2012).

11. Lee, A. S.-Y., Burdeinick-Kerr, R. & Whelan, S. P. A ribosome-specialized translation initiation pathway is required for cap-dependent translation of vesicular stomatitis virus mRNAs. *Proceedings of the National Academy of Sciences* **110**, 324–329 (2013).

12. Tiruneh, B. S., Kim, B.-H., Gallie, D. R., Roy, B. & von Arnim, A. G. The global translation profile in a ribosomal protein mutant resembles that of an eIF3 mutant. *BMC biology* **11**, 123 (2013).

13. Ramagopal, S. & Ennis, H. L. Regulation of synthesis of cell-specific ribosomal proteins during differentiation of *Dictyostelium discoideum*. *Proceedings of the National Academy of Sciences* **78**, 3083–3087 (1981).

14. Ramagopal, S. Induction of cell-specific ribosomal proteins in aggregation-competent non-morphogenetic *Dictyostelium discoideum*. *Biochemistry and Cell Biology* **68**, 1281–1287 (1990).

15. Parenteau, J. *et al.* Introns within ribosomal protein genes regulate the production and function of yeast ribosomes. *Cell* **147**, 320–331 (2011).

16. Slavov, N. & Botstein, D. Coupling among growth rate response, metabolic cycle, and cell division cycle in yeast. *Molecular Biology of the Cell* **22**, 1997–2009 (2011).

17. O'Leary, M. N. *et al.* Tthe ribosomal protein Rpl22 controls ribosome composition by directly repressing expression of its own paralog, Rpl22l1. *PLoS genetics* **9**, e1003708 (2013).

18. Wool, I. G. Extraribosomal functions of ribosomal proteins. *Trends in biochemical sciences* **21**, 164–165 (1996).

19. Warner, J. R. & McIntosh, K. B. How common are extraribosomal functions of ribosomal proteins? *Molecular cell* **34**, 3–11 (2009).

20. Reschke, M. *et al.* Characterization and analysis of the composition and dynamics of the mammalian riboproteome. *Cell Reports* **4**, 1276–1287 (2013).

21. Slavov, N., Budnik, B., Schwab, D., Airoldi, E. & van Oudenaarden, A. Constant Growth Rate Can Be Supported by Decreasing Energy Flux and Increasing Aerobic Glycolysis. *Cell Reports* **7**, 705 – 714 (2014).

22. Bantscheff, M., Schirle, M., Sweetman, G., Rick, J. & Kuster, B. Quantitative mass spectrometry in proteomics: a critical review. *Analytical and bioanalytical chemistry* **389**, 1017–1031 (2007).

23. Sykes, M. T., Shajani, Z., Sperling, E., Beck, A. H. & Williamson, J. R. Quantitative proteomic analysis of ribosome assembly and turnover *In Vivo*. *Journal of molecular biology* **403**, 331–345 (2010).

24. Noll, H., Staehelin, T. & Wettstein, F. Ribosomal aggregates engaged in protein synthesis: ergosome breakdown and messenger ribonucleic acid transport. *Nature* **198**, 632–638 (1963).

25. Wettstein, F., Staehelin, T. & Noll, H. Ribosomal aggregate engaged in protein synthesis: characterization of the ergosome. *Nature* **197**, 430–435 (1963).

26. Qian, W., Ma, D., Xiao, C., Wang, Z. & Zhang, J. The genomic landscape and evolutionary resolution of antagonistic pleiotropy in yeast. *Cell Reports* **2**, 1399–1410 (2012).

27. Shalem, O. *et al.* Genome-scale CRISPR-Cas9 knockout screening in human cells. *Science* **343**, 84–87 (2014).

Figure 1 | The stoichiometry among core RPs in yeast ribosomes depends both on the number of ribosomes per mRNA and on the physiological condition. **a**, Sucrose gradients allow separating ribosomes that are free or bound to a single mRNA (monosomes) from multiple ribosomes bound to a single mRNA (polysomes). The absorbance at 254 nm reflects RNA levels, mostly ribosomal RNA. The vertical dashed lines indicate the boundaries of the collected fractions. **b**, Fold-changes estimated by MS are plotted against the fold-changes expected from the amount of universal proteomics standard (UPS2) added to sucrose fractions. All fold-changes are relative to the first data point, and the error bars are coefficients of variation. The fitted line has a slope of 0.88, indicating about 12% systematic underestimation. **c**, Levels of core RPs in the sucrose fractions estimated from their unique peptides quantified by MS (Extended Data Fig. 1, Supplementary Methods and Discussion). The RP levels vary depending on the carbon source (glucose or ethanol) and on the number of ribosomes bound per mRNA, indicated with the Roman numbers in parenthesis; Glu (i) indicates monosomes from glucose carbon source, Eth (iii) indicates trisomes from ethanol carbon source and so on. **d**, The pattern of the relative levels of RPs without paralogs is similar to the pattern for all RPs shown in panel (c). **e**, The levels of the L37 paralogs (Rpl37ap and Rpl37bp) are negatively correlated while the levels of the L17 paralogs (Rpl17ap are Rpl17bp) are positively correlated. **f**, Correlations between the levels of paralogous RPs computed as in panel (e). In all panels, RP levels are plotted on $\log_2$ scale relative to the mean levels across all fractions.

Figure 2 | The stoichiometry among core RPs in mouse ribosomes depends on the number of ribosomes per mRNA. a, Sucrose gradients allow separating ribosomes that are free or bound to a single mRNA (monosomes) from multiple ribosomes bound to a single mRNA (polysomes). The absorbance at 254 nm reflects RNA levels, mostly ribosomal RNA. The vertical dashed lines indicate the boundaries of the collected fractions. **b**, The levels of core RPs in monosomes and polysomes were quantified by MS and found to vary depending on the number of ribosomes bound per mRNA, indicated with the Roman numbers in parenthesis. The first and the second columns display data for the same sample labeled with different tandem-mass-tags (reporter ions 126 or 131) as a control. The levels of each RP are shown on a $\log_2$ scale relative to the mean level across all fractions. **c**, The $\log_2$ ratios between polysomal and monosomal levels of mouse RPs are plotted against the corresponding $\log_2$ ratios between the polysomal and monosomal levels of their orthologous yeast RPs. The significant (p-value < 0.03) positive correlation between these ratios suggests that the RP-stoichiometry differences are conserved across yeast and mouse. The plot includes all orthologous RP pairs with over 65% sequence identity between yeast and mouse.

Figure 3 | The relative levels of RPs across monosomes and polysomes correlate significantly to the fitness of yeast and mammalian cells lacking the genes encoding these RPs. a, The fitnesses of RP–deleted yeast strains[26] are inversely proportional (p–value $< 4 \times 10^{-3}$) to the relative levels of the corresponding RPs in tetra–ribosomes; both the fitness and the RP-levels are for yeast growing on ethanol carbon source. The RPs without paralogs are marked with green squares. **b-c**, Extension of the analysis in panel (a) to all conditions: correlations between the relative RP levels from Fig. 1c and the fitnesses (either in glucose or in ethanol carbon source) of strains lacking the corresponding RP genes[26]. The correlations are shown either for all quantified RPs (**b**) or only for RPs without paralogs (**c**). **d**, The distribution of sequence identity between human RPs and their closest mouse orthologs; the sequences and annotations for RPs are from Swiss–Prot. **e**, Extension of the analysis for yeast in panels (a-c) to mouse: correlations between the relative levels of mouse RPs from Fig. 2b and the fitnesses of human ESC lacking the corresponding human ortholog[27]. The correlations are shown either for all quantified RPs or only for RPs whose sequence identity between mouse and human exceeds 80 %. Error bars are standard deviations.

Acknowledgments We thank P. Vaidyanathan for help with the sucrose gradients and S. Kryazhimskiy, W. Gilbert, P. Vaidyanathan, G. Frenkel, and A. Murray for discussions and constructive comments. This work was funded by a grant from the National Institutes of Health to A.v.O. (R01-GM068957) and Alfred P Sloan Research Fellowship to E.M.A.

Competing Interests The authors declare that they have no competing financial interests.

Contributions N.S., S.S. and B.B. performed experiments and collected data. N.S., A.v.O. and E.A. analysed the data. N.S. and A.v.O. discussed the results and wrote the manuscript.

Figure 1

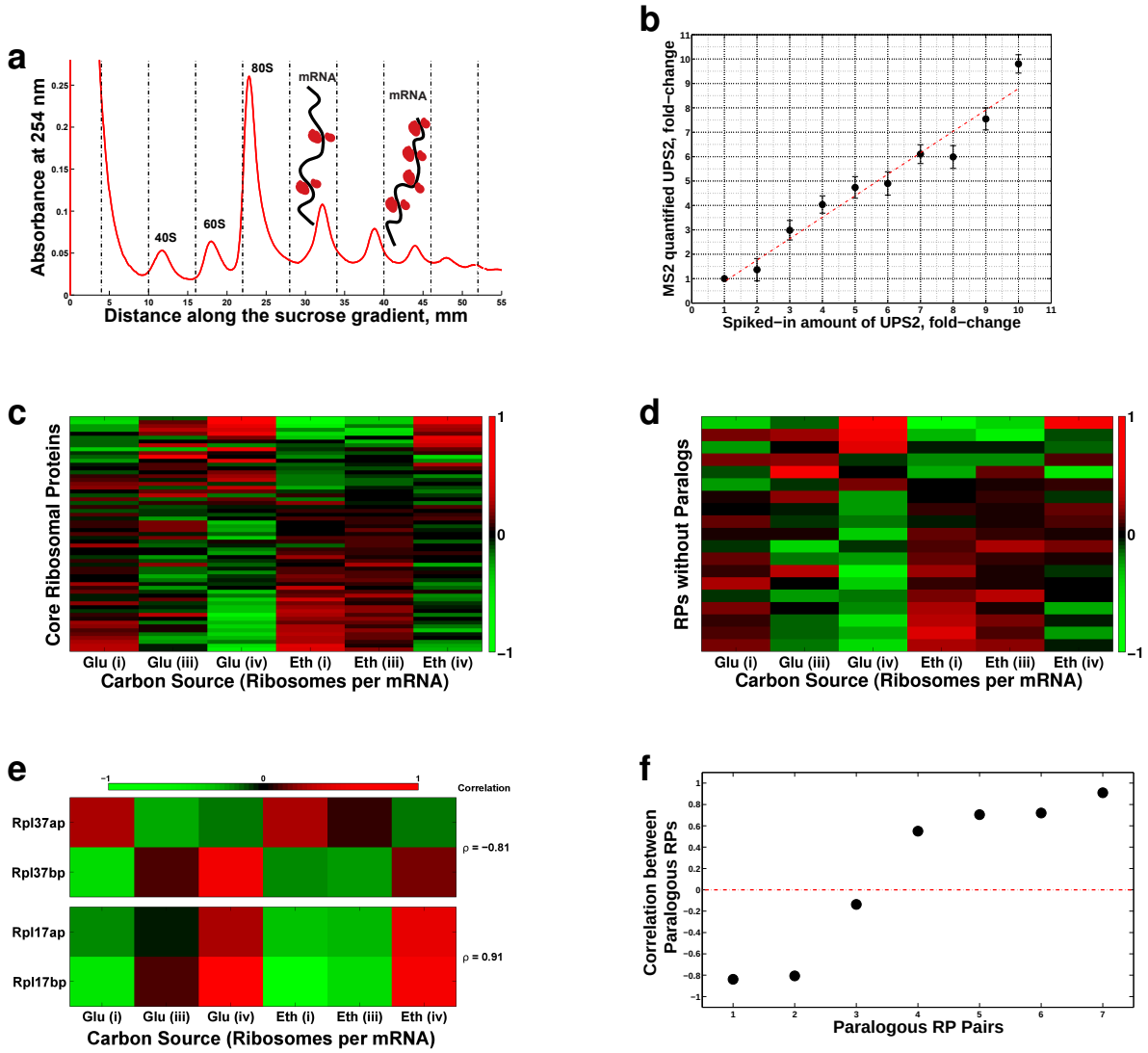
a
Absorbance at 254 nm
40S
60S
80S
mRNA
mRNA
Distance along the sucrose gradient, mm
b
MS2 quantified UPS2, fold−change
Spiked−in amount of UPS2, fold−change
c
Core Ribosomal Proteins
Glu (i) Glu (iii) Glu (iv) Eth (i) Eth (iii) Eth (iv)
Carbon Source (Ribosomes per mRNA)
d
RPs without Paralogs
Glu (i) Glu (iii) Glu (iv) Eth (i) Eth (iii) Eth (iv)
Carbon Source (Ribosomes per mRNA)
e
Correlation
Rpl37ap
Rpl37bp
ρ = −0.81
Rpl17ap
Rpl17bp
ρ = 0.91
Glu (i) Glu (iii) Glu (iv) Eth (i) Eth (iii) Eth (iv)
Carbon Source (Ribosomes per mRNA)
f
Correlation between Paralogous RPs
Paralogous RP Pairs

Figure 2

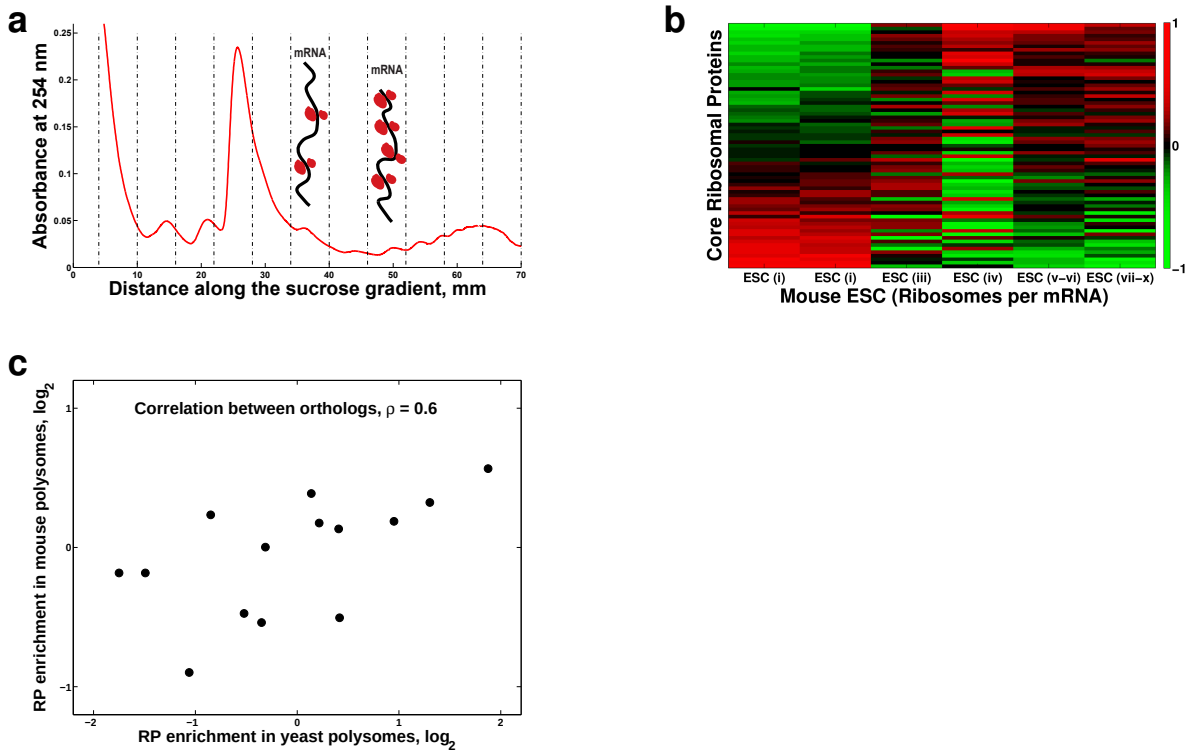
a
Absorbance at 254 nm
mRNA
mRNA
Distance along the sucrose gradient, mm
b
Core Ribosomal Proteins
ESC (i)
ESC (i)
ESC (iii)
ESC (iv)
ESC (v–vi)
ESC (vii–x)
Mouse ESC (Ribosomes per mRNA)
c
Correlation between orthologs, ρ = 0.6
RP enrichment in mouse polysomes, log2
RP enrichment in yeast polysomes, log2

Figure 3

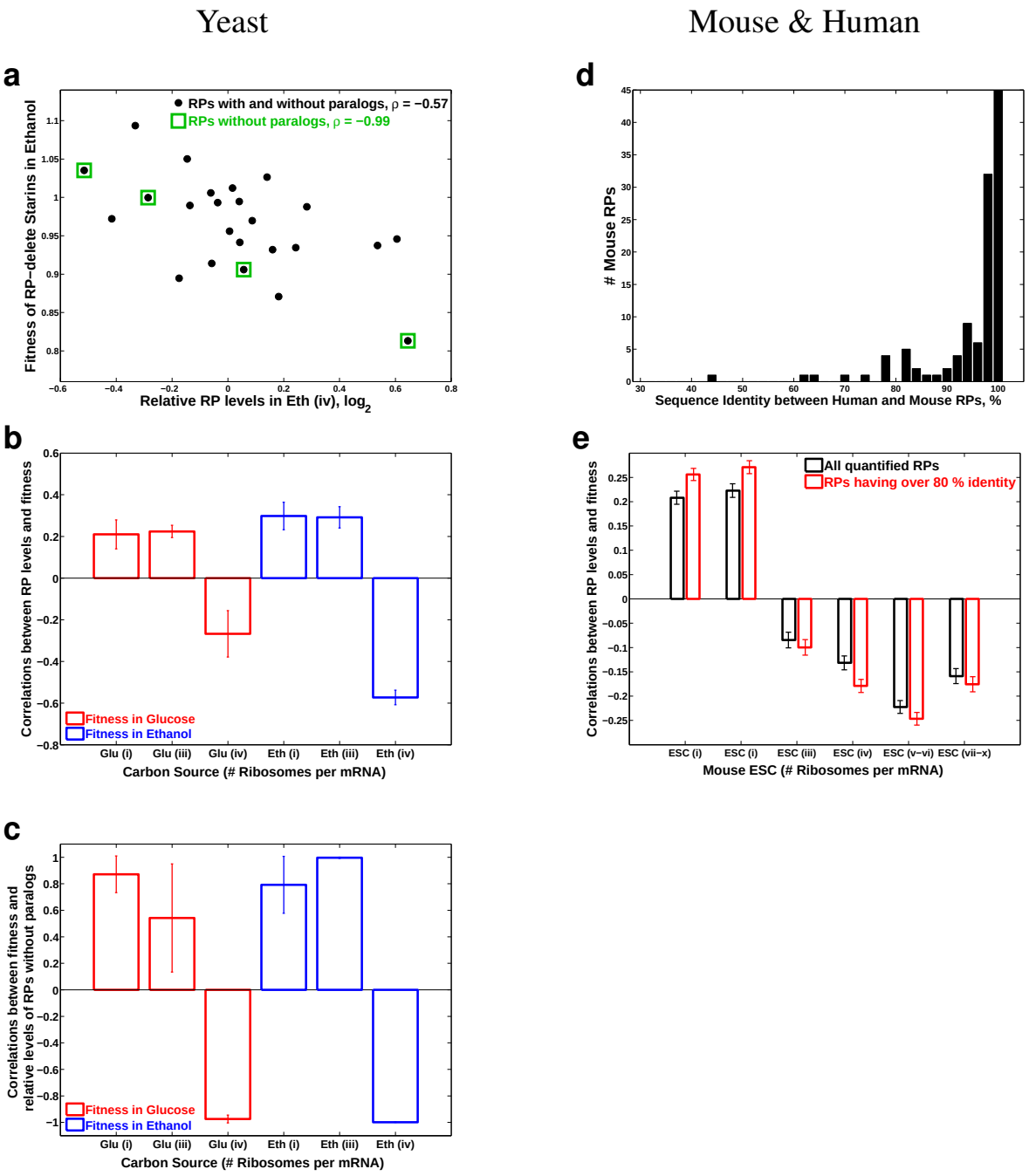
Yeast
Mouse & Human
a
RPs with and without paralogs, ρ = −0.57
RPs without paralogs, ρ = −0.99
Fitness of RP−delete Starins in Ethanol
Relative RP levels in Eth (iv), log2
d
Mouse RPs
Sequence Identity between Human and Mouse RPs, %
b
Correlations between RP levels and fitness
Fitness in Glucose
Fitness in Ethanol
Glu (i)
Glu (iii)
Glu (iv)
Eth (i)
Eth (iii)
Eth (iv)
Carbon Source (# Ribosomes per mRNA)
e
All quantified RPs
RPs having over 80 % identity
Correlations between RP levels and fitness
ESC (i)
ESC (i)
ESC (iii)
ESC (iv)
ESC (v−vi)
ESC (vii−x)
Mouse ESC (# Ribosomes per mRNA)
c
Correlations between fitness and relative levels of RPs without paralogs
Fitness in Glucose
Fitness in Ethanol
Glu (i)
Glu (iii)
Glu (iv)
Eth (i)
Eth (iii)
Eth (iv)
Carbon Source (# Ribosomes per mRNA)

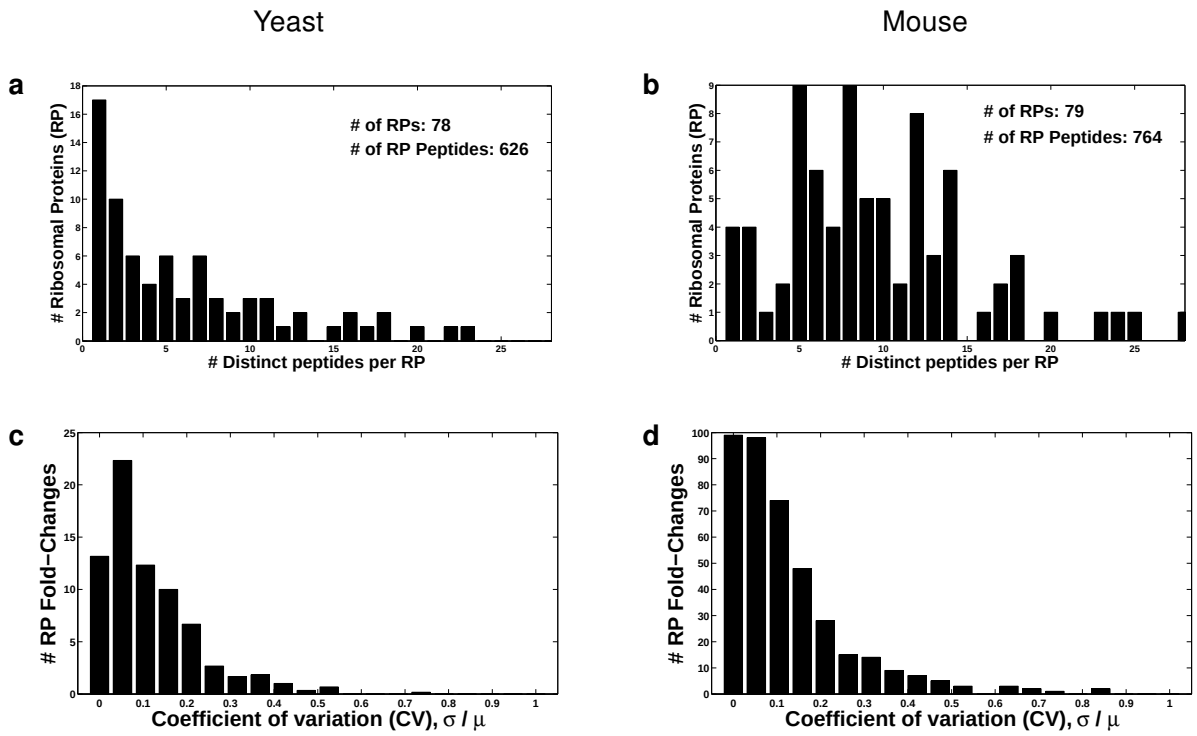

Extended Data Figure 1 | **Multiple unique peptides per RP provide consistent fold-change estimates for most RPs.** **a**, Number of unique peptides quantified per RP in yeast. **b**, Number of unique peptides quantified per RP in mouse. **c**, Distribution of coefficients of variation (CVs) of the measured fold-changes for yeast RPs. The CVs for each RP quantify the consistency of fold-changes for that RP estimated from all quantified unique peptides whose amino acid sequences are found only in the RP and no other protein in the proteome. CVs are estimated as the standard deviation (σ) of the fold-changes of unique peptides mapping to the same RP over the corresponding mean (μ) and are thus computed only for RPs that have multiple unique peptides. **d**, Distribution of CVs of the measured fold-changes for mouse RPs. See Supplementary Discussion for details.

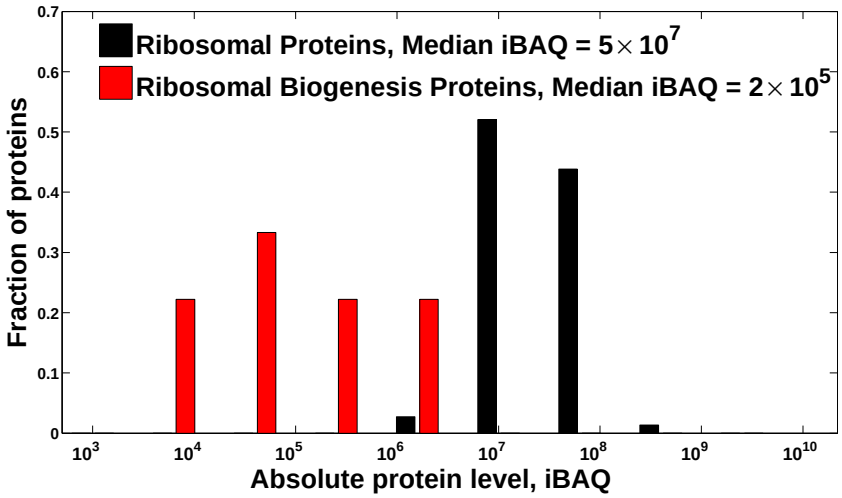

Extended Data Figure 2 | **RPs are over 100 fold more abundant that ribosome biogenesis proteins in the sucrose gradients.** Distributions of iBAQ scores for RPs and for ribosome biogenesis proteins. The iBAQ score of a protein estimates its absolute level based on the number of unique peptides for that proteins and their corresponding integrated precursor areas. The levels of ribosome biogenesis proteins likely reflect the levels of the 90S preribosomal particles in our sucrose gradients. See Supplementary Discussion and Supplementary Methods for details.

Supplementary Information

Supplementary Methods

Cultivation of yeast

All yeast experiments used a prototrophic diploid strain (DBY12007) with a S288c background and wild type HAP1 alleles[1]. We grew our cultures in a commercial bioreactor (LAMBDA Laboratory Instruments) using minimal media with the composition of yeast nitrogen base (YNB) and supplemented with $2g/L$ D-glucose. Before inoculation, the reactor was filled with 2L of minimal media and warmed up to a working temperature of 30^oC. Then cultures were started by inoculating the media with 100 μl overnight culture from DBY12007. The overnight cultures were prepared by first streaking frozen DBY12007 on YPD plates (YPD; 10 g of Bacto-Yeast extract, 20 g of Bacto-peptone, 20 g of Bacto-agar, and 20 g of glucose in 1000 ml of water) and then growing a single colony in the same minimal media used for the subsequent growth experiment in the bioreactor. The density of the culture used for inoculation was 2×10^7 cells per ml, resulting in initial density of 10^3 cells/ml for the culture in the reactor. The cultures were grown at 30^oC and continuously stirred to ensure their homogeneity. The culture was aerated with air coming

from a compressed gas cylinder (Airgas, AI-B300 breathable air). The incoming flow of air was controlled by a thermal-based mass-flow controller and filtered through a $0.2\mu m$ filter to ensure sterility.

Cell density was measured on Beckman-Coulter Multisizer 4 by counting of at least 20,000 single cells[2,3]. The samples were taken during the first exponential growth phase on glucose carbon source and during the second exponential growth phase on ethanol[4]. To take samples without disturbing the cultures, we used a metal tube attached to a silicon tubing and a syringe. The metal tube could be inserted in and out of the cultures, and the syringe used to sample the required volume quickly from the homogeneous cultures. The sampling tubing was kept sterile and no culture was left in it after sampling. All samples were immediately filtered, frozen in liquid nitrogen and processed as described below.

Cultivation of mouse ESC

Mouse embryonic stem cells (E14 10^{th} passage) were grown as adherent cultures in 10 cm plates with 10 ml DMEM/F12 media supplemented with 10 % knockout serum replacement, nonessential amino acids (NEAA supplement), 0.1 mM β-mercapto-ethanol, 1 % penicillin/streptomycin, leukemia inhibitory factor (LIF; 1,000 U LIF/ml), and $2i$ (GSK3β and Mek 1/2 inhibitors). Cultures were started at a cell density of 10^5 cells/ml and passaged every other day with accutase. The cells grew exponentially with a growth rate of about 0.07 per hour. At cell density of 6×10^5 cells/ml, the cells were detached from the plate by 2 min incubation with accutase (Millipore) at

$37\ ^oC$. The cells were pelleted by a 2 min centrifugation and the pellet frozen immediately in liquid nitrogen.

Sucrose gradients and mass spectrometry work flow

Both yeast and mouse embryonic stem cells were lysed by vortexing for 10 min with glass beads in cold PLB (20 mM HEPES-KOH at pH 7.4, 1 % Triton X–100, 2 mM Magnesium Acetate, 100 mM Potassium Acetate, 0.1 mg/ml cycloheximide, and 3 mM DTT). The crude extracts obtained from this lysis procedure were clarified by centrifugation and the resulting supernatants were applied to linear 11 ml sucrose gradients ($10\ \% - 50\ \%$) and spun at 35,000 rpm in a Beckman SW41 rotor either for 3 hours (for yeast samples) or for 2.5 hours (for mouse samples). Twelve fractions from each sample were collected using a Gradient Station (BioComp, Cat. # 153-001). The RNA profile across the gradient was measured by Gradient Profiler (BioComp).

Sample preparation

The proteins from each sucrose fraction were purified by methanol-chloroform precipitation and the amount of protein estimated by the dry weight of the purified proteins. To ensure full dissociation of the ribosomes, each sucrose fraction was mixed with 4 volumes of 8 M Guanidinium chloride and vortexed for at least 10 min.

To provide a standard for evaluating the accuracy of protein quantification, we spiked-in a known amount of the universal proteomics standard (UPS2). A 100 μg of total protein from

each sucrose fraction were mixed with: (i) a predetermined amount of UPS2 whose cysteines were alkylated either with vinylpyridine and (ii) a predetermined amount of UPS2 whose cysteines were alkylated with iodoacetamide. The quantification of UPS2 in Fig. 1b is derived only from the cysteine containing peptides alkylated with iodoacetamide. The mixtures of yeast proteins from the sucrose fractions and UPS2 proteins were digested using slightly modified FASP protocol[5]. Subsequently each time-point-sample was labeled with TMT reagent (Prod # 90061, Thermo Fisher, San Jose, CA) according to the manufacturer's protocol.

Tandem Mass Tags (TMT) mass spectrometry

The labeled set–sample was injected from an auto–sampler into the trapping column ($75\ \mu m$ column ID, 5 cm packed with $5\ \mu m$ beads on 20 nm pores, from Michrom Bioresources, Inc.) and washed for 15 min; the sample was eluted to analytic column with a gradient from 2 to 32 % of buffer B (0.1 % formic acid in ACN) over $180\ min$ gradient and fed into TLQ Orbitrap Elite (Thermo Fisher, San Jose, CA). The instrument was set to run in TOP 20 MS/MS mode method with dynamic exclusion. After MS1 scan in Orbitrap with 30K resolving power, each ion was submitted to an HCD MS/MS with 15K or 30K resolving power and to CID MS/MS scan subsequently. All quantification data were derived from HCD spectra.

Analysis of mass spectrometry spectra

Mass/charge spectra where analyzed by MaxQuant[6] (version 1.4.1.2), SEQUEST HT[7] and Mascot[8] (Version 2.4.1) run via the Proteome Discover (64bit version 1.4.0.288, Thermo), and standalone

Mascot. All searches were run on a Windows server 2008 64 bit operating system with 64 CPU blades and 256 GB of RAM with the following general parameters. Parent ion mass tolerance was set to 20 ppm, mass tolerance for MS/MS ions was set to 0.02 Da for HCD and to 0.6 Da for CID spectra. For all searches, minimal peptide length was specified as 6 amino acids and maximal peptide length as 50 amino acids. The peptide charge state was limited to +7 for searches with MaxQuant. Searches were performed against either the yeast or the mouse uniprot database and common contaminants that were added to the database. Searches had trypsin enzyme specificity, allowing 2 missed cleavages. Asn and Gln deamidation and Met oxidation were included as variable modifications in the search parameters.

The search results from all search engines were filtered at 1 % false discovery rate (FDR) on both protein and on peptide levels using the Percolator (Version 2.05 Build Date May 6 2013). The results exported for further analysis included all peptide spectrum matches (PSM) that were assigned to one or more proteins and passed the statistical significance filter. These results were outputted in the "Evidence File" for MaxQuant and in a peptide–level–results text file for Proteome Discover.

Correlation between relative RP levels and fitness

To explore the physiological significance (if any) of the altered RP stoichiometry, we computed the correlation between the fitness of yeast strains with single RP-gene deletions[9] and the corresponding relative RP levels that we measured (Fig. 3). In yeast, 21 pairs of RP-genes encode

proteins with identical amino acid sequence within a pair. Since the RP proteins within these 21 pairs cannot be distinguished by MS, these 21 RPs were excluded from our analysis and not used to compute correlations between RP levels and fitness of RP-delete strains. Furthermore, some RPs that we quantified did not have RP-deletion fitness data and thus could not be included in our correlation analysis.

Supplementary Discussion

Evaluation of factors that may affect the measured RP levels

The estimated RP levels (Fig. 1c, Fig. 2b) appear to vary significantly between monosomes and polysomes and across the growth conditions. However, this variation might reflect not only stoichiometry changes among the RPs but also other factors and artifacts, such as noise in the MS measurements, a differential distribution of nascent RP polypeptides among monosomes and polysomes, posttranslational modifications (PTMs) of the RPs and the presence 90S ribosomal biogenesis particles. In the subsections below we describe our investigation of such potential artifacts. The results of this investigation (Extended Data Fig. 1 and Extended Data Fig. 2), indicate that such potential artifacts are unlikely to contribute significantly to the estimated RP levels (Fig. 1c and Fig. 2b), suggesting that the stoichiometry among the RPs can change across polyribosomes and physiological conditions in the absence of genetic perturbations.

Noise, coisolation interference and posttranslational modifications (PTMs)

From most RPs, we quantify multiple unique peptides (whose amino acid sequence is found only in one RP and no other protein in the proteome) both in yeast (Extended Data Fig. 1a) and in mouse (Extended Data Fig. 1b). In the absence of measurement noise, post-translational modifications (PTMs) or partial peptides (such as nascent poly-peptide chains), the fold changes of a RP should equal the fold change of each unique peptide coming from this RP. Thus the similarity between the fold changes of unique peptides for the same RP, as quantified by the coefficient of variation (CV; the ratio of the standard deviation to the mean), reflects the degree to which the estimated fold-changes for RP are influenced by post-posttranslational modification, by noise, and by partial protein products. To evaluate the contribution of all these factors to our RP quantification (Fig. 1c, Fig. 2b), we computed the distributions of CV values for yeast (Extended Data Fig. 1c) and for mouse (Extended Data Fig. 1d) for all RPs with more than 1 unique peptide per RP. These distributions indicate a median CV < 0.15 and thus suggest that PTMs, measurement noise and partial RPs are not dominant factors in the quantification of most RPs. A few fold-changes, however, have larger CVs that might reflect either PTMs or larger noise in the peptide quantification.

Coisolation interference in the quantification of the reporter ions results in underestimation of the fold changes[10]. To reduce the influence of coisolation interference, we filtered out the quantified peptides with large oisolation interference. We used only peptides with less than $10 - 30\%$ coisolation interference[4,11] for quantifying RPs and the spiked-in universal proteomics standard (UPS2) proteins. The estimated fold-changes of the UPS2 proteins correspond closely with the

fold-changes expected based on the spiked-in amount of the UPS2 standard (Fig. 1b).

Differential distribution of nascent RP polypeptides among monosomes and polysomes

A differential distribution of nascent RP polypeptides among monosomes and polysomes could contribute to the measured RP changes (Fig. 1c and Fig. 2b). As discussed above, the low CVs for protein fold changes quantified from different unique peptides (Extended Data Fig. 1c-d) make this possibility unlikely.

We sought to test the possibility that nascent RP polypeptides contribute to our estimates of RP levels even more directly. If nascent RPs contribute significant number of peptides to the variation in RP levels in Fig. 1c and Fig. 2b, the MS1 precursor-area (integrated area under the MS1 spectrum of the precursor ions that reflects peptide abundance) of N-terminal peptides would be higher compared to the MS1 precursor-area of C-terminal peptides. We compared the distributions of MS1 precursor-areas for N-terminal peptides and for C-terminal peptides and found that the two distributions are statistically identical both for yeast and for mouse. This result indicates that nascent RPs do not contribute significantly to the measured changes in the RP stoichiometry.

The 90S ribosomal biogenesis particles

Sucrose gradients separate not only mature ribosomes but also other cellular organelles of comparable size, such as the immature 90S ribosomal biogenesis particles[12–15]. The 90S particles should have unequal distribution across the gradient, localizing closely to the 80S monosomal

peak and decreasing toward the higher sedimentation-velocity region of of the polysomes. Thus if the amount of 90S particles is comparable to the amount of ribosomes, 90S particles could contribute significantly to the changes in the RP stoichiometry in Fig. 1c and Fig. 2b. However in exponentially growing cells, the 90S ribosomal biogenesis particles are less abundant than the mature ribosomes[12–15], and thus unlikely to contribute large fraction to the RP peptides that we quantified.

We used our data to evaluate the extent to which immature 90S particles contribute to our estimates of variability among the RPs. Two key factors that determine this contribution are (i) the level and (ii) the sucrose-gradient localization of the 90S. To estimate these two factors, we used the ribosomes biogenesis proteins that are known to be associated with the 90S particle but not with the mature ribosomes[12]. These ribosomes biogenesis proteins provide a solid basis for estimating the abundance of the 90S particles relative to the mature ribosomes and the distribution of the 90S particles across the sucrose fractions.

First, we estimated the abundance of the 90S particle relative to the mature ribosomes. From the 180 proteins annotated by the gene ontology (GO:0042254) term "ribosome biogenesis", we have quantified unique peptides for only 14 proteins that are not core structural RPs. These 14 ribosome-biogenesis proteins are represented in our data by very few peptides (9 proteins are represented by a single peptide), which likely reflects the low abundance of these proteins (relative to the RPs) in our sucrose fractions. This conclusion is strongly supported by the low MS1 precursor-area (integrated area under the MS1 spectrum of the precursor ions) of ribosome-biogenesis pep-

tides compared to the MS1 precursor-area of RP peptides. To obtain a more quantitative estimate for the abundance of 90S relative to the mature ribosomes, we computed and compared the iBAQ scores[16] (a popular measure for absolute protein levels) for the RPs and for the ribosome biogenesis proteins. The iBAQ scores indicate that the detected ribosome biogenesis proteins and thus the 90S particles are about 100 times less abundant than the RPs and thus the mature ribosomes (Extended Data Fig. 2), consistent with previous observations[14]. Therefore, the proteins derived from the 90S can contribute about $1\ \%$ to the RP fold-changes in Fig. 1c. Since many of the measured RP fold-changes exceed $100\ \%$, 90S particles are unlikely to contribute significantly to the variation in the ribosome stoichiometry that we measured.

Second, as expected the 90S ribosome biogenesis peptides are localized to the 80S monosomal fraction and their levels are even lower and constant across the rest of the sucrose gradient. Thus their small contribution is limited to the monosomes and cannot account for the relative RP changes across polysomes that we observed both in yeast and in mouse (Fig. 1c and Fig. 2b).

Stoichiometry among RPs

Our data show that while the levels of some RPs increase, the levels of other RPs decrease. These opposite trends indicate that the ratios (stoichiometries) among RPs making-up monosomes and polysomes vary. However, our population–average measurements do not indicate the number of distinct ribosomes in each sucrose fraction or the exact RP composition of such distinct ribosomes.

RPs of the small (40S) and the large (60S) subunits are about equally represented among the

subset of RPs that increase or decrease across monosomes and polysomes. Therefore, preferential enrichment of 40S or 60S in some fractions is very unlikely to contribute to the variation among RPs that we observe.

1. Hickman, M. & Winston, F. Heme levels switch the function of Hap1 of *Saccharomyces cerevisiae* between transcriptional activator and transcriptional repressor. *Molecular and Cellular Biology* **27**, 7414–7424 (2007).

2. Slavov, N., Macinskas, J., Caudy, A. & Botstein, D. Metabolic cycling without cell division cycling in respiring yeast. *Proceedings of the National Academy of Sciences of the United States of America* **108**, 19090–19095 (2011).

3. Slavov, N. & Botstein, D. Coupling among growth rate response, metabolic cycle, and cell division cycle in yeast. *Molecular Biology of the Cell* **22**, 1997–2009 (2011).

4. Slavov, N., Budnik, B., Schwab, D., Airoldi, E. & van Oudenaarden, A. Constant Growth Rate Can Be Supported by Decreasing Energy Flux and Increasing Aerobic Glycolysis. *Cell Reports* **7**, 705 – 714 (2014).

5. Wiśniewski, J., Zougman, A., Nagaraj, N. & Mann, M. Universal sample preparation method for proteome analysis. *Nature methods* **6**, 359–362 (2009).

6. Cox, J. & Mann, M. Maxquant enables high peptide identification rates, individualized ppb-range mass accuracies and proteome-wide protein quantification. *Nature biotechnology* **26**, 1367–1372 (2008).

7. Eng, J. K., McCormack, A. L. & Yates Iii, J. R. An approach to correlate tandem mass spectral data of peptides with amino acid sequences in a protein database. *Journal of the American Society for Mass Spectrometry* **5**, 976–989 (1994).

8. Cottrell, J. & London, U. Probability-based protein identification by searching sequence databases using mass spectrometry data. *Electrophoresis* **20**, 3551–3567 (1999).

9. Qian, W., Ma, D., Xiao, C., Wang, Z. & Zhang, J. The genomic landscape and evolutionary resolution of antagonistic pleiotropy in yeast. *Cell Reports* **2**, 1399–1410 (2012).

10. Bantscheff, M., Schirle, M., Sweetman, G., Rick, J. & Kuster, B. Quantitative mass spectrometry in proteomics: a critical review. *Analytical and bioanalytical chemistry* **389**, 1017–1031 (2007).

11. Altelaar, A. *et al.* Benchmarking stable isotope labeling based quantitative proteomics. *Journal of proteomics* **88**, 14–26 (2013).

12. Granneman, S. & Baserga, S. J. Ribosome biogenesis: of knobs and rna processing. *Experimental cell research* **296**, 43–50 (2004).

13. Sykes, M. T. & Williamson, J. R. A complex assembly landscape for the 30S ribosomal subunit. *Annual review of biophysics* **38**, 197–215 (2009).

14. Sykes, M. T., Shajani, Z., Sperling, E., Beck, A. H. & Williamson, J. R. Quantitative proteomic analysis of ribosome assembly and turnover *In Vivo*. *Journal of molecular biology* **403**, 331–345 (2010).

15. Chen, S. S. & Williamson, J. R. Characterization of the ribosome biogenesis landscape in *E. coli* using quantitative mass spectrometry. *Journal of molecular biology* **425**, 767–779 (2013).

16. Schwanhäusser, B. *et al.* Global quantification of mammalian gene expression control. *Nature* **473**, 337–342 (2011).